Optics Letters

# Vector modulation instability in gas-filled multi-pass cells

Esmerando Escoto,[1,*] Andrea Zablah,[1] Supriya Rajhans,[1] Xavier Délen,[2] Marc Hanna,[2] and Christoph M. Heyl[1,3,4]

[1]Deutsches Elektronen-Synchrotron DESY, Notkestraße 85, 22607 Hamburg, Germany
[2]Université Paris-Saclay, Institut d'Optique Graduate School, CNRS, Laboratoire Charles Fabry, 91127 Palaiseau, France
[3]Helmholtz Institute Jena, Fröbelstieg 3, 07743 Jena, Germany
[4]GSI Helmholtzzentrum für Schwerionenforschung GmbH, Planckstraße 1, 64291 Darmstadt, Germany
*esmerando.escoto@desy.de

Received 2 June 2026; revised 9 July 2026; accepted 11 July 2026; posted 13 July 2026; published 27 July 2026

**Multi-pass cells (MPCs) have emerged as versatile systems for nonlinear pulse compression supporting large single-stage compression factors. However, their performance is limited at extreme B-integrals by the onset of secondary nonlinear effects, which lead to the appearance of parasitic spectral peaks. In this Letter, we report the experimental observation of vector modulation instability (VMI) as a primary limiting mechanism in gas-filled MPCs operating at B-integrals >30 radians. The VMI signal is polarized orthogonally to the input beam and distinct from spectral features arising due to quasi-phase-matched four-wave mixing (QPM-FWM). We experimentally show that the VMI gain scales with accumulated B-integral, rather than with only gas density or peak power. Crucially, employing a circularly polarized input pulse suppresses VMI. This mitigation strategy, combined with dispersion management, is confirmed via simulations as a way for single-stage compression factors to exceed 40.** 

https://doi.org/10.1364/OL.607420

Ytterbium (Yb)-based laser systems have become a workhorse for high-average-power ultrafast applications. However, due to their limited emission bandwidth, these lasers are generally limited to durations of several hundred femtoseconds. To reach the lower femtosecond or even few-cycle regime required for advanced ultrafast applications, efficient nonlinear post-compression is essential. Multi-pass cells (MPCs) have emerged as a powerful tool for achieving the required high compression factors within a single stage or using cascaded stages. Their design is simple, yet highly effective, typically consisting of two concave mirrors and a nonlinear medium, either a noble gas or a transparent bulk material. Figure 1 gives a comprehensive overview of several state-of-the-art MPC systems compiled from recent literature [1–31]. While most single-stage MPC systems deliver compression factors between 15 and 25, a few notable outliers approach 40.

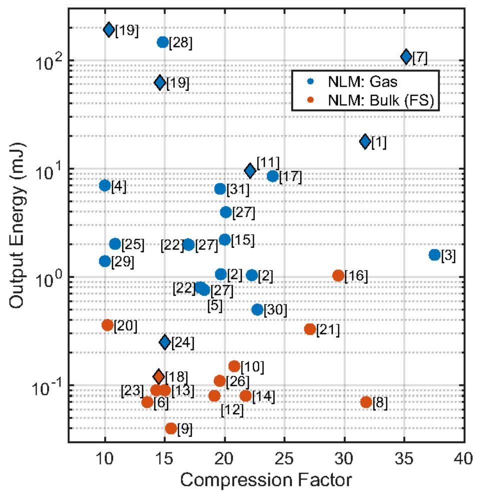


**Fig. 1.** Summary of reported single-stage MPC post-compression systems, using gas (blue) or bulk material (red) as nonlinear medium (NLM). Marked with ∘ are systems where the full power is compressed, while ⋄ used only an attenuated beam for compression.

Pushing toward these record compression values fundamentally requires accumulating a large nonlinear phase shift. The maximum achievable compression in a single cell is often initially constrained by practical factors: the pressure limits of the gas vessel, bulk material thickness (before self-focusing dominates), or the damage threshold of the optics. While these are often mitigated by scaling the cell geometry or switching nonlinear media, a more fundamental limitation arises at very high B-integrals: secondary nonlinear effects result in the appearance of parasitic spectral peaks. These peaks were first reported in MPCs by Kaumanns *et al.* [1], who reached a compression factor of 32 ($B > 50$ radians), and were later reported by Rußbüldt *et al.* [2] and Koltalo *et al.* [28] at factors around 20 ($B > 30$ radians). Because the B-integral $B$ scales linearly with the maximum compression factor, these effects become unavoidable when attempting to reach record compression values. Initially attributed to ionization in [1], the mechanism is later described as a quasi-phase-matched four-wave mixing (QPM-FWM) process, driven by the periodic nature of the nonlinear interactions and dispersion within the MPC [32].

In this Letter, we discuss a different nonlinear effect observed in MPCs operating at extreme B-integrals: vector modulation instability (VMI). We show the emergence of spectral peaks caused by VMI, occurring at a polarization perpendicular to that of the linearly polarized input beam. We observe VMI together with QPM-FWM, albeit with different scaling properties. By systematically varying the gas pressure in the MPC chamber, we demonstrate that the VMI gain is fundamentally driven by the total accumulated B-integral rather than independently by gas density or peak input power. Furthermore, we experimentally demonstrate how VMI can be mitigated. Finally, if QPM-FWM can also be suppressed, we show via simulations that it is possible to push single-stage compression factors beyond the current records reported in Fig. 1.

Modulation instability (MI) is a fundamental nonlinear phenomenon arising from the interplay between optical nonlinearity and dispersion during wave propagation. Under suitable conditions, small-amplitude fluctuations, originating from technical or quantum noise, experience gain over a finite frequency range and evolve into symmetric spectral sidebands, drawing energy from the central frequency. While traditional scalar MI requires anomalous dispersion, VMI represents another form of instability that readily occurs in the normal-dispersion regime, driven fundamentally by cross-phase modulation (XPM) between orthogonal polarization states [33,34]. Even when the input beam is nominally linearly polarized, fluctuations or slight depolarization can seed an orthogonal polarization component. Under extreme nonlinear accumulation, XPM induces exponential growth of this perpendicular component. QPM-FWM observed in MPCs is analogous to MI in dispersion-oscillating fibers [35], where periodicity allows MI to occur even in the absence of anomalous dispersion.

Adapting the derivation from [36] considering non-birefringent materials, the VMI gain $g(\omega)$ can be expressed as:

$$g(\omega) = |\beta_2| \sqrt{\omega^2 \left( \frac{4\gamma P_o}{3|\beta_2|} - \omega^2 \right)}, \tag{1}$$

where $\beta_2$ is the group-velocity dispersion, $\gamma = n_2 k_o / A_{\mathrm{eff}}$ is the nonlinear coefficient, and $P_o$ is the peak power. In the case of a MPC, $\beta_2$ and $\gamma$ are averaged over one roundtrip [37]. The peak gain occurs symmetrically at the frequencies:

$$\omega_{\max} = \pm \sqrt{\frac{2\gamma P_o}{3|\beta_2|}}, \tag{2}$$

yielding a maximum gain value of $g_{\max} = 2\gamma P_o/3$. This reveals that for gas-filled MPCs, the peak gain value $g_{\max}$ scales linearly with the accumulated B-integral ($\equiv \int_0^L \gamma P_o dz$). Furthermore, as shown in Eq. (2), the spectral position of this peak gain $\omega_{\max}$ is independent of the gas pressure. Because both the nonlinear parameter $\gamma$ and the dispersion $\beta_2$ scale linearly with gas density, their ratio remains constant, effectively canceling out the dependence on the cell's operating pressure.

To confirm these VMI characteristics, we experimentally study the onset of VMI using an argon-filled MPC. The experimental setup, depicted in Fig. 2, was specifically designed to detect onset and parameter scaling of VMI. The driving source is a Ytterbium-based laser delivering 1-ps pulses centered at 1030 nm, operating at 40 kHz repetition rate. To systematically

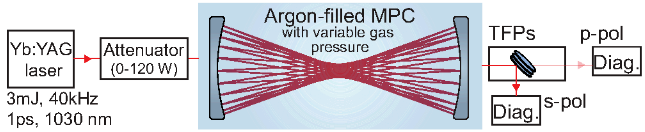


**Fig. 2.** Experimental setup. Diag.: diagnostics, each consisting of a power meter and a spectrometer. TFPs: thin-film polarizers.

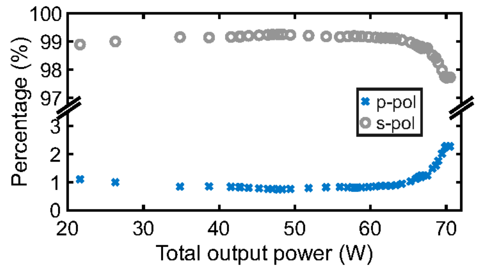


**Fig. 3.** Measured output powers from the MPC filled with argon at 3 bar. A sudden power transfer from s- to p-polarized signal at high power, with the input beam being s-polarized, indicates the onset of VMI.

vary the accumulated B-integral without altering the input pulse duration or spatial profile of the laser, the input power is controlled using an attenuator, consisting of a half-wave plate and a polarizer, capable of tuning the average power up to 120 W (corresponding to pulse energies up to 3 mJ).

The linear (s-polarized) input beam is sent into the gas-filled MPC using a mode-matching telescope (MMT) designed to achieve an approximately equal spot size on the MPC mirrors for all beam passes through the MPC. The MPC comprises two concave mirrors with a 500 mm radius of curvature, housed within a sealed chamber designed for stable operation across various gas pressures up to about 4 bar. After propagating through 26 roundtrips inside the MPC, the spectrally broadened output is recollimated and directed into a high-contrast polarization diagnostic setup. Accurately characterizing VMI requires detecting a very weak p-polarized signal emerging from a predominantly s-polarized background. To achieve the necessary extinction ratio, the beam is split using a series of three cascaded thin-film polarizers (TFPs). Each TFP individually reflects 99.5% of the s-polarized light and transmits 95.0% of the p-polarized light. The separated beams are then simultaneously routed to power meters and silicon-based spectrometers to monitor the onset of depolarization along with spectral features.

Using 3 bars of argon in the MPC chamber, the input power is increased until a limit of spectral broadening is reached, which is observed at about 65 W total output power, corresponding to approximately $B = 45$ rad. The limit is observed in different ways simultaneously: the beam suddenly flickers and becomes unstable, while the spectrum stops broadening as parasitic spectral peaks appear. Monitoring the total power distributed between the s- and p-polarized outputs reveals the physical mechanism behind this limit (Fig. 3). At lower input powers, the output remains s-polarized, similar to the input. However, as the total output power exceeds approximately 65 W, a sudden depolarization occurs. This sharp threshold behavior is characteristic of an exponential gain process like VMI, which rapidly diverts significant optical power from the primary s-polarized pump into the initially unseeded p-polarized mode.

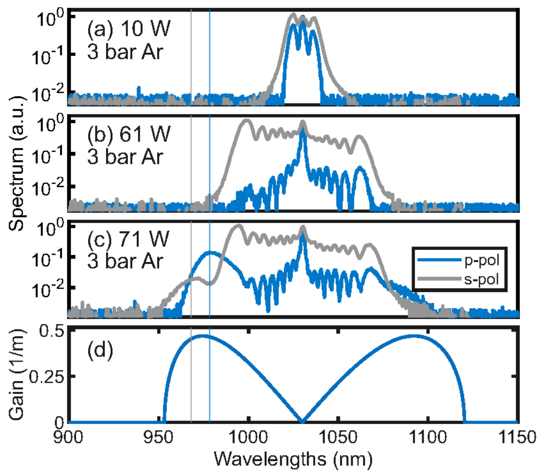


**Fig. 4.** Measured MPC output spectra for s- and p-polarization, with 3 bars of argon in the MPC. The locations of the spectral peaks in (c) located outside the SPM-broadened spectrum at 968 nm and 979 nm are marked with two vertical lines in all panels. The VMI gain computed using Eq. (1) is shown in (d).

The measured spectra of the s- and p-polarized outputs are shown in Fig. 4. In both spectra, peaks separate from the self-phase modulation (SPM) spectrum can be observed. The theoretically predicted VMI peak gain position shown in Fig. 4(d) aligns remarkably well with the experimentally measured p-polarized peak shown in Fig. 4(c). The spectral peak appearing in the s-polarized output (the input polarization axis) can be attributed to QPM-FWM [32]. It should be noted that the spectrometers utilized in this setup are silicon-based, featuring a sharp drop in quantum efficiency near 1100 nm. In addition, the p-polarized transmission of the TFPs is >95% only between 980 and 1080 nm, and reduces to <10% outside the range of 940 to 1120 nm. Consequently, the long-wavelength VMI and likewise the QPM-FWM peaks are barely visible. Also, due to the limited extinction ratio, some parts of the input beam still leak through, appearing in wavelengths where no gain is expected.

Equation (2) predicts the frequency at which VMI reaches its peak gain to scale with the square root of the peak power $P_o$. However, the peak gain value scales linearly with the B-integral, meaning the peaks should be visible at different power levels when the gas pressure is changed. To observe this, the pressure in the MPC chamber is changed to different values: 4, 3.5, 3, and 2.5 bars of argon, and the power is again increased until the spectral broadening limit discussed before is observed. Note that the limit is based on visual observation; hence, the total B-integral for each case is slightly different. The results are shown in Fig. 5. As expected, while the peaks emerge at progressively higher average powers for lower gas pressures, they appear at the same accumulated B-integral, indicated by the same amount of SPM spectral broadening achieved for all cases. Furthermore, the spectral positions of the VMI peaks only shift slightly further from the central wavelength due to the $\sqrt{P_o}$ dependence. This is in contrast to the behavior of QPM-FWM peaks visible in the s-polarized measurements: because phase-matching conditions are highly sensitive to gas dispersion, the QPM-FWM peaks shift drastically in wavelength and change in amplitude as the gas pressure is changed. This is evident from the QPM condition, $\Delta\beta L + B = 2m\pi$, where $m$ is an integer, $B$ is the B-integral per

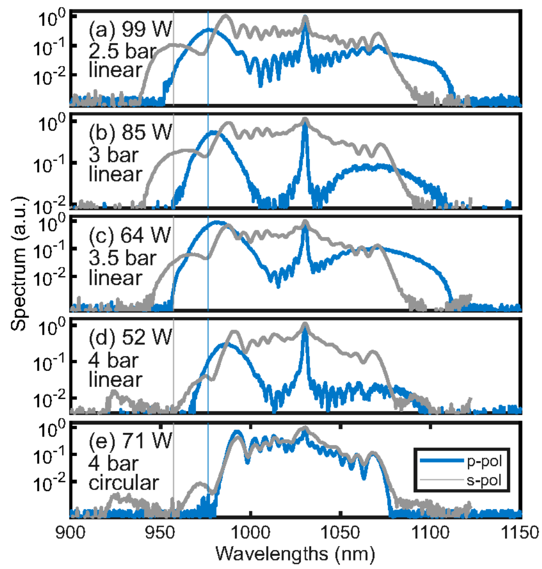


**Fig. 5.** Measured MPC output spectra for the s- and p-polarization at (a) 2.5 bars, (b) 3 bars, (c) 3.5 bars, and (d) 4 bars of argon, and with an average power tuned to the onset of VMI for each gas pressure. The spectral position of the peaks in (a) located at 957 nm and 977 nm, is marked in all panels by two vertical lines. The spectra in (e) correspond to the same gas pressure as in (d) of 4 bars but using a circularly polarized input.

pass and $\Delta\beta \equiv \beta(\omega_s) + \beta(\omega_i) - 2\beta(\omega_p)$ with the subscripts signifying the signal, idler, and pump frequencies. Note that the occurrence of MPC output beam instability and additional spectral peaks was also interpreted as multi-photon ionization and/or plasma generation in the past [1]. However, since the discussed effects occur at very different peak power levels as shown in Fig. 5 (the corresponding peak focus intensity ranges from 0.8 to $1.5 \times 10^{13}$ W/cm$^2$), a strongly intensity-dependent process like ionization does not seem to play a role.

As established in fiber optics [33], VMI driven by cross-phase modulation can be suppressed by using a circularly polarized input beam. To test this mitigation strategy, a quarter-waveplate was used to generate a circularly polarized input. In this case, higher input power is needed to achieve the required B-integral, since a circularly polarized beam has a lower effective nonlinear refractive index compared to the linear case. With different input powers, the same amount of broadening is achieved in the two cases shown in Figs. 5(d) and 5(e), although in the latter case, the VMI signal disappeared. However, while VMI is avoided, QPM-FWM peaks in Fig. 5(e) are still prominently observed, matching with Fig. 5(d), as the phase matching conditions of the two cases are very similar. The difference between the two spectra in Fig. 5(e), with the QPM-FWM peaks more prominent only in s-polarization, can be explained by the limited p-polarized transmission of the TFPs beyond 980-1080 nm. While circular polarization solves the VMI limitation, further spectral broadening also requires suppression of QPM-FWM.

As QPM-FWM requires dispersion between the input pulse and the FWM emission bands [32], suppression of QPM-FWM can be expected if the MPC is operated close to zero dispersion across the bandwidth supported by the MPC. Using a hybrid pulse propagation model described in [32] but adapted to include polarization vectors, we simulate the case in Fig. 4, with

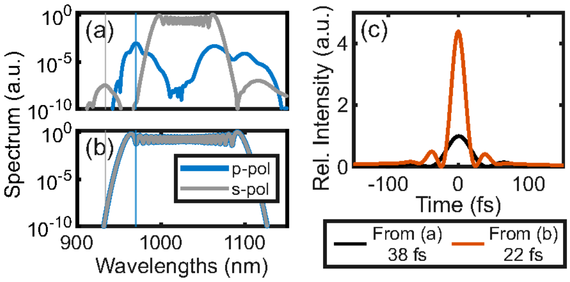


**Fig. 6.** (a) Simulation of MPC spectral broadening using the experimental parameters reported in Fig. 4. (b) Output spectra obtained using a circularly polarized input pulse, 5 bars of argon, and mirrors with −50 fs$^2$. (c) Corresponding compressed pulses by group-delay dispersion optimization.

linearly polarized input and 3 bars of argon similar to the experiment. The simulated output spectra are shown in Fig. 6(a). The QPM-FWM peak is marked with the vertical line at 934 nm and the VMI peak at 970 nm. In the case shown in Fig. 6(b), the MPC mirrors compensate for a dispersion of −50 fs$^2$. In this case, parasitic spectral peaks are not observed. The small residual dispersion translates into a QPM-FWM peak gain being shifted outside of the mirror reflectivity bandwidth, and using circular polarization clearly eliminates VMI. This allows us to increase the input power further to 100 W while increasing the gas pressure to 5 bars, resulting in a compression factor of more than 40, reaching beyond current records summarized in Fig. 1. Spectral broadening is now mainly limited by the bandwidth of the dielectric mirrors, which in both the experiment and this simulation reflect >99.5% only between 950 and 1120 nm.

In conclusion, we have presented the first observation of VMI in gas-filled MPCs and identified this process as a fundamental mechanism that limits spectral broadening at extreme B-integrals. Our experimental results demonstrate that the VMI gain is inherently dependent on the accumulated B-integral. This could be confirmed by the emergence of strong, cross-polarized parasitic peaks at the same degree of spectral broadening across varying pressures of argon. Furthermore, we verified that switching to circularly input polarization successfully suppresses the onset of VMI. However, even with VMI mitigated, QPM-FWM continues to restrict the maximum achievable broadening in current setups. To overcome this remaining limitation, our simulations indicate that designing MPC mirrors to compensate for the dispersion accumulated within the gas effectively suppresses QPM-FWM. By eliminating the effects of both VMI and QPM-FWM, our simulations indicate the possibility to compress 1-ps pulses to durations below 25 fs, a single-stage compression factor greater than 40, which would significantly surpass the capabilities of demonstrated MPC systems.

**Funding.** Deutsche Forschungsgemeinschaft (545612524); Bundesministerium für Forschung, Technologie und Raumfahrt (13N16678); Agence Nationale de la Recherche (ANR-24-CE92-0010-02 MILLSTREAMS).

**Acknowledgment.** We acknowledge Class 5 Photonics GmbH for the use of their facilities to do the experiments reported in this Letter.

**Disclosures.** The authors declare no conflicts of interest.

**Data availability.** Data underlying the results presented in this paper are not publicly available at this time but may be obtained from the authors upon reasonable request.

## REFERENCES

1. M. Kaumanns, V. Pervak, D. Kormin, *et al.*, Opt. Lett. **43**, 5877 (2018).
2. P. Rußbüldt, J. Weitenberg, J. Schulte, *et al.*, Opt. Lett. **44**, 5222 (2019).
3. P. Balla, A. Bin Wahid, I. Sytcevich, *et al.*, Opt. Lett. **45**, 2572 (2020).
4. P. L. Kramer, M. K. Windeler, K. Mecseki, *et al.*, Opt. Express **28**, 16951 (2020).
5. A.-L. Viotti, S. Alisauskas, A. Bin Wahid, *et al.*, J. Synchrotron. Radiat. **28**, 36 (2021).
6. M. Seidel, P. Balla, T. Binhammer, *et al.*, in *EPJ Web of Conferences*, Vol. **243** (EDP Sciences, 2020), p. 21001.
7. M. Kaumanns, D. Kormin, T. Nubbemeyer, *et al.*, Opt. Lett. **46**, 929 (2021).
8. M. Seidel, P. Balla, C. Li, *et al.*, Ultrafast Sci. **2022**, 9754919 (2022).
9. J. Song, Z. Wang, X. Wang, *et al.*, Chin. Opt. Lett. **19**, 093201 (2021).
10. Y. Pfaff, C. Forster, G. Barbiero, *et al.*, Opt. Express **30**, 10981 (2022).
11. J. Song, L. Shen, J. Sun, *et al.*, Opt. Express **30**, 24276 (2022).
12. M. Seidel, F. Pressacco, O. Akcaalan, *et al.*, Laser Photonics Rev. **16**, 2100268 (2022).
13. A.-L. Viotti, C. Li, G. Arisholm, *et al.*, Opt. Lett. **48**, 984 (2023).
14. A.-L. Viotti, S. Alisauskas, M. Seidel, *et al.*, Rev. Sci. Instrum. **94**, 023002 (2023).
15. X. Zhang, Z. Wang, X. Wang, *et al.*, Chin. Phys. B **32**, 104206 (2023).
16. S. Rajhans, E. Escoto, N. Khodakovskiy, *et al.*, Opt. Lett. **48**, 4753 (2023).
17. J. Song, Y. Peng, G. Luo, *et al.*, Appl. Phys. B **129**, 86 (2023).
18. Y. Pfaff, G. Barbiero, M. Rampp, *et al.*, Opt. Express **31**, 22740 (2023).
19. A. Omar, M. Hoffmann, G. Galle, *et al.*, Opt. Express **32**, 13235 (2024).
20. L. Shen, J. Song, Y. Peng, *et al.*, IEEE Photonics Technol. Lett. **36**, 1257 (2024).
21. J.-F. Hergott, F. Réau, N. Lericheux, *et al.*, in *EPJ Web of Conferences*, Vol. **309** (EDP Sciences, 2024), p. 07002.
22. E. Escoto, F. Pressacco, Y. Jiang, *et al.*, Opt. Lett. **49**, 6841 (2024).
23. G. Beaufort, N. Jimenez, V. Hariton, *et al.*, in *EPJ Web of Conferences*, Vol. **307** (EDP Sciences, 2024), p. 04038.
24. Z. Hu, K. Fritsch, and O. Pronin, "Supercontinuum generation in the low-peak-power regime using a single-stage multipass cell," arXiv (2025).
25. J. Guo, L. Guo, Z. Gao, *et al.*, Opt. Lett. **49**, 4385 (2024).
26. P. Biesterfeld, A. Schönberg, M. Seitz, *et al.*, J. Phys. Photonics **8**, 015013 (2026).
27. J.-F. Hergott, F. Réau, O. Tcherbakoff, *et al.*, Appl. Phys. B **131**, 56 (2025).
28. V. Koltalo, L. Daniault, C. Sire, *et al.*, in *Ultrafast Optics UFO XIV* (2025), paper M2.7.
29. B. Gilicze, I. Seres, Z. Bengery, *et al.*, High Power Laser Sci. Eng. **13**, e104 (2025).
30. G. Cichelli, G. Parize, M. Natile, *et al.*, Opt. Lett. **50**, 6714 (2025).
31. A. Schönberg, S. Rajhans, E. Escoto, *et al.*, Photonics Res. **13**, 761 (2025).
32. M. Hanna, N. Daher, F. Guichard, *et al.*, J. Opt. Soc. Am. B **37**, 2982 (2020).
33. G. P. Agrawal, in *Nonlinear Fiber Optics*, 5th ed. (Academic Press, 2013), p. 193.
34. G. Millot, E. Seve, S. Wabnitz, *et al.*, J. Opt. Soc. Am. B **15**, 1266 (1998).
35. A. Mussot, M. Conforti, S. Trillo, *et al.*, Adv. Opt. Photonics **10**, 1 (2017).
36. S. Wabnitz, Phys. Rev. A **38**, 2018 (1988).
37. N. Daher, F. Guichard, S. W. Jolly, *et al.*, J. Opt. Soc. Am. B **37**, 993 (2020).